Bessel functions $I_m(z)$ [(A2); Abramowitz & Stegun (1966)]:

$$\int \exp(-q^2x^2)\exp[ip(x+\lambda)]\,dx = (\pi^{1/2}/q)\exp[-p^2/(4q^2)]\cos p\lambda \quad (A1)$$

$$\exp(z\cos\theta) = \sum \exp(im\theta) I_m(z). \quad (A2)$$

References

ABRAMOWITZ, M. & STEGUN, I. A. (1966). *Handbook of Mathematical Functions.* Washington, DC: National Bureau of Standards.

ANDERSON, S., HYDE, S. T. & VON SCHNERING, H. G. (1984). *Z. Kristallogr.* **168**, 1-17.

DUNSTETTER, F. (1988). Thèse d'Etat, Univ. de Paris Sud, France.

DUNSTETTER, F. & DELAPALME, A. (1989). *Physica (Utrecht)*, **B156 & 157**, 112-114.

EINSTEIN, A. (1907). *Ann. Phys. (Leipzig)*, **22**, 180-190.

FISCHER, W. & KOCH, W. (1989). *Acta Cryst.* A**45**, 166-169, 485-490, 726-732.

GRADSHTEYN, I. S. & RYZHIK, I. W. (1965). *Tables of Integrals, Series and Products.* New York: Academic Press.

JOHNSON, C. K. (1969). *Acta Cryst.* A**25**, 187-194.

JOHNSON, C. K. & LEVY, H. A. (1974). In *International Tables for X-ray Crystallography*, Vol. IV. Birmingham: Kynoch Press. (Present distributor Kluwer Academic Publishers, Dordrecht.)

KOCH, E. & FISCHER, W. (1989). *Acta Cryst.* A**45**, 169-174, 553-563.

PATTERSON, A. L. (1952). *Acta Cryst.* **5**, 829-833.

PRANDL, W. (1981). *Acta Cryst.* A**37**, 811-818.

PRANDL, W. & DUNSTETTER, F. (1992). Submitted to *Acta Cryst.*

PRESS, W. H., FLANNERY, B. P., TEUKOLSKY, S. A. & VETTERLING, W. T. (1986). *Numerical Recipes.* Cambridge Univ. Press.

SCHNERING, H. G. VON & NESPER, R. (1987). *Angew. Chem.* **95**, 1097-1230.

VOGT, K. & PRANDL, W. (1983). *J. Phys. C*, **16**, 4753-4768.

WILLIS, B. T. M. & PRYOR, A. W. (1975). *Thermal Vibrations in Crystallography.* Cambridge Univ. Press.

Acta Cryst. (1992). A**48**, 180-188

Accuracy in Laue X-ray Diffraction Analysis of Protein Structures

BY H. D. BARTUNIK, H. H. BARTSCH AND HUANG QICHEN*

Max-Planck-Society, Research Unit for Structural Molecular Biology, c/o DESY, Notkestrasse 85, 2000 *Hamburg* 52, *Germany*

(*Received* 7 *May* 1991; *accepted* 12 *August* 1991)

Abstract

The accuracy in protein structure analysis based on Laue X-ray diffraction has been investigated for the example of two orthorhombic structures of bovine pancreatic trypsin (BPT). The precision in the Laue structure factors and the contrast in electron-density maps were used as criteria. A comparison with the results of previous analyses based on conventional crystal rotation methods showed that high resolution around 1.4 Å may be reached with both monochromatic and polychromatic techniques. Electron-density maps exhibited significantly lower contrast when calculated on the basis of Laue structure amplitudes, due to inefficient exploration of reciprocal space at low resolution by the Laue method even in the case of a broad bandwidth and inclusion of exposures from several different crystal orientations. Laue data were recorded on photographic film and processed using the program *LAUEMAD* [Bartunik & Borchert (1989). *Acta Cryst.* A**45**, 718-726]. The empirically derived wavelength scaling factors based on a comparison of equivalent reflection intensities were in good agreement with theoretical estimates over a broad wavelength range. One BPT structure was refined on the basis of Laue structure amplitudes (current R factor 24% at 1.8 Å resolution).

Introduction

Laue diffraction techniques using synchrotron radiation permit the recording of a large number of simultaneously excited reflections during short exposure times. This provides a means for investigating enzyme kinetics and protein dynamics based on crystal structure analysis of transient states (Moffat, Szebenyi & Bilderback, 1984; Helliwell, 1985; Hajdu, Acharya, Stuart, Barford & Johnson, 1988; Hajdu & Johnson, 1990). A first application of this method to structural analysis of an enzyme reaction intermediate with a lifetime of several minutes has recently been reported (Schlichting, Rapp, John, Wittinghofer, Pai & Goody, 1989). Even much shorter time scales are within reach. In the case of well diffracting crystals of medium-size protein structures such as trypsin, lysozyme or myoglobin, exposure times in the range of 1-10 ms suffice to obtain Laue diffraction patterns extending to atomic resolution at presently operational storage rings (*e.g.* Moffat, 1989; Bartunik, 1991). In addition

* Present address: Institute of Physical Chemistry, Peking University, Beijing, People's Republic of China.

0108-7673/92/020180-09$03.00

to short exposure times, a number of further conditions have to be fulfilled for analysis of short-lived structural states by Laue techniques. The conformational transitions must be initiated by external stimulation using, for example, laser chemistry (Bartunik, 1983). High population of an intermediate over the whole crystal volume has to be reached; this problem and possible solutions have been discussed elsewhere (*e.g.* Moffat, 1989; Bartunik, 1991).

In cases where cyclic repetition of the reaction is not feasible, such as in enzyme kinetics on short time scales, all diffraction data needed for structural analysis would have to be measured at a minimum number of different crystal orientations. This raises the question of how completeness in Laue structure-factor sets may be reached. Of particular concern is the systematic lack of completeness at low resolution, which is characteristic for Laue methods and its effect on the contrast in electron-density maps. Further, the application of broad-bandpass Laue techniques relies on the preservation of high crystalline order during the reaction under investigation. Diffraction to medium resolution may be sufficient for following changes in the relative orientation of domains, *e.g.* in enzymatic reactions of kinases. Such large-amplitude motions however will often cause a strong broadening in the crystal mosaic spread so that only reduced-bandpass Laue techniques are applicable (Bartunik & Borchert, 1989). Studies of conformational changes involving only motions of small amplitudes aim to determine reliably the distances between specific interacting atoms and groups of atoms, hence atomic resolution and high contrast in electron-density maps will be required. Assuming that sufficiently accurate start phases are known, the success of such studies will essentially depend on the accuracy and completeness in the Laue structure amplitude set. The present study has been undertaken mainly in order to investigate the power of Laue methods for such applications.

This study is based on Laue diffraction-data collection to high resolution from orthorhombic bovine pancreatic trypsin (BPT). The data were processed with the program package *LAUEMAD* (Bartunik & Borchert, 1989). One of the BPT structures was refined at 1.8 Å resolution on the basis of Laue structure amplitudes. The relative accuracy of monochromatic and polychromatic techniques was studied by comparing the contrast in electron-density maps.

Laue data collection

BPT crystals were grown in the presence of benzamidine as described previously (Bode & Schwager, 1975; Bartunik, Summers & Bartsch, 1989). Two different orthorhombic forms were used in the present studies. Both forms belong to the space group $P2_12_12_1$. One form ('HTN1'; pH 5.3) has cell dimensions $a = 63.6$, $b = 63.5$, $c = 67.8$ Å. Crystals of the second form ('TP 9') were grown at pH 6.8 and transferred to pH 9.0 a short time before the Laue exposures were taken. The change in pH to a value above the pK of histidine was undertaken in order to compare the TP 9 structure to a previously determined BPT structure ('DEBA') at pH 8.0 belonging to the same space group. DEBA was refined at 1.45 Å (Marquart, Walter, Deisenhofer, Bode & Huber, 1983), the BPT-HTN1 structure at 1.50 Å resolution (Bartunik, Summers & Bartsch, 1989; Protein Data Bank entry 1TLD). For both the HTN1 and TP 9 forms, crystals with a size of about $0.4 \times 0.4 \times 0.8$ mm were used.

One series of Laue diffraction experiments was carried out on the bending magnet beamline X31/EMBL which includes a double-focusing Au-coated quartz mirror providing 1:1 imaging (Bartunik, Fourme & Phillips, 1982; Bartunik & Borchert, 1989). The short-wavelength cutoff was near 0.6 Å. DORIS was running at 5.2 GeV with maximum electron currents around 40 mA. The incident-beam cross section was limited to 100×100 μm. The divergence in the incident beam was *ca* 1.2 arc min in the vertical and 2.3 arc min in the horizontal direction. In another series of experiments, Laue data were collected on the 20-pole wiggler beamline W2/HASYLAB using a simple pin-hole geometry. The beam aperture was 0.2 mm; the divergence in the incident beam was about 0.2 arc min in the vertical and 0.55 arc min in the horizontal direction. An aluminium absorber limited the wavelength range in the incident beam to $\lambda \leq 1.6$ Å. On the short-wavelength side, diffraction spots were visible for exciting wavelengths $\lambda \geq 0.25$ Å.

Diffraction patterns were recorded on photographic film (CEA) using four films per film pack. For each crystal orientation, two subsequent exposures were taken with different exposure times in order to optimize conditions for low- and high-resolution reflection intensities, respectively. Typical exposure times varied between 0.1 and 0.5 s (W2) and 1 and 10 s (X31). A shutter system was used consisting of a chopper with adjustable opening times ≥ 100 μs and a conventional electromagnetically driven shutter preventing frame overlap (Koelln, 1990). Up to ten pairs of high- and low-resolution exposures were recorded at different crystal orientations from fresh parts of the same BPT crystal. All BPT crystals were suitable for white-beam Laue experiments, *i.e.* their crystal mosaicities were so small that the observed reflection spots did not show any streaking. The films were digitized into 8 bits using an Optronics scanner with a raster size of 50 μm.

Laue data processing and crystal structure analysis

The Laue data were processed with the program package *LAUEMAD* (Bartunik & Borchert, 1989) which

is partly based on *MADNES* (Messerschmidt & Pflugrath, 1987). *LAUEMAD* assumes a spherical resolution function or *Intensitätsbereich* (von Laue, 1960) in reciprocal space, thus taking into account an effective isotropic crystal mosaicity. A detailed description of the procedures employed by *LAUEMAD* has been given by Borchert (1989).

Simultaneously excited reflections

The percentage of all independent reflections ('completeness') which can be measured simultaneously depends on the orientation of the crystal relative to the incident beam. The completeness was estimated in a series of simulation calculations for BPT Laue data collection on station X31 (assuming a wavelength range $0.68 < \lambda < 1.6$ Å, a crystal-to-film distance of 85 mm, a film size of 5×5 in, a collimator aperture of 100 μm and a pixel resolution of 50 μm). Fig. 1 shows the results of the predictions. As expected, the highest percentage of simultaneously observable independent reflections from an orthorhombic BPT crystal is obtained when all principal axes are inclined relative to the incident beam. However, the maximum value does not exceed about 35%. The dependence of the completeness of the data set on the crystal orientation is also clearly visible in the experimental results (Fig. 2).

A part of the simultaneously excited reflections overlaps in energy (harmonics) or spatially. The percentage of multiply excited reflections was estimated on the basis of theoretical multiplicity distributions (Cruickshank, Helliwell & Moffat, 1987). For the Laue data collection on station X31 using a wavelength range with $M = \lambda_{max}/\lambda_{min} \simeq 3$, about 88% of all excited reflections are singlets, less than 9% doublets and the rest higher multiplets. For the Laue data recorded on station W2 ($M \simeq 8$), 85% are singlets and 10% doublets. Because of the relatively high percentage of singlets and the lower accuracy which is expected in structure amplitudes derived from multiplets, only singlets were included in the present study.

Orientation matrix determination and refinement

The crystal orientation relative to the incident beam was determined on the basis of 'nodal spot' positions corresponding to superpositions of multiplets. Based on a comparison of predicted and observed nodals, an improved orientation matrix was derived by *LAUEMAD*. The range of convergence was about 5° in the initial misorientation angles. In this first step, the accuracy in the crystal orientation matrix corresponded to typically 0.5 pixel in the reflection spot positions.

In a subsequent step, the orientation matrix was refined together with the crystal parameters (cell dimensions, effective mosaic spread) and experimental parameters (crystal-to-detector distance, detector orientation relative to the incident beam). The simultaneous refinement of these parameters involved an 'eigenvalue filtering' procedure (Reeke, 1984; Bricogne, 1986).

The typical size of reflections present on the Laue exposures of BPT corresponded to 8×8 pixels. Determination of an approximate crystal orientation involved application of the dynamical mask option (see below) on the basis of 'packed' patterns averaged over 4×4 pixels. After refinement of the experimental parameters, the crystal orientation matrix and the cell constants, the calculated and observed reflection positions agreed within 14–54 μm (Table 1). In the refinement of the cell constants, an accuracy of typically 0.15–0.20% was achieved.

As an alternative approach, we determined an approximate crystal orientation matrix on the basis of low-indexed zonal curves for an entirely unknown

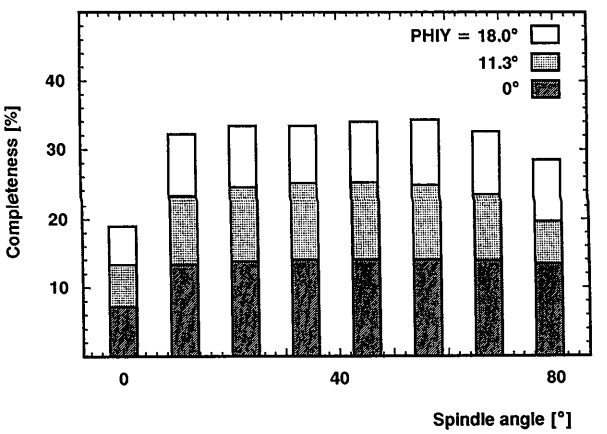

Fig. 1. Predicted completeness *vs* crystal orientation for the BPT-TP 9 structure. The crystal is stepwise rotated through an angle PHI around the *a* axis. (90° – PHIY) denotes the inclination of the *a* axis relative to the incident beam.

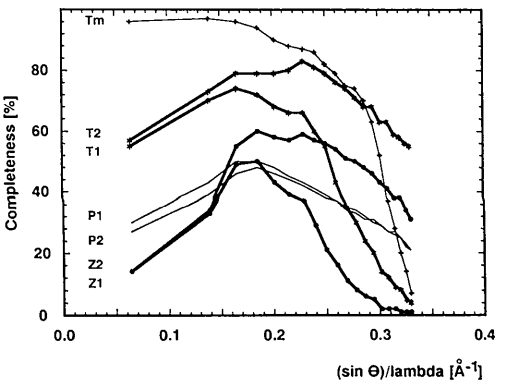

Fig. 2. Completeness of processed Laue structure-factor sets *vs* $(\sin\theta)/\lambda$. T1 (GOOD reflections) and T2 (GOOD, WEAK): data for TP 9 (see Table 1). Z1 (GOOD) and Z2 (GOOD, WEAK): HTN1 at PHIY = 0. Tm: monochromatic DEBA structure factors. P1 (for PHI = 42°/PHIY = 36°) and P2 (56°/18°): predictions under optimized crystal orientations.

Table 1. *Processing of BPT-TP 9 Laue data*

Resolution:	$d > 1.5$ Å.
Wavelength range:	0.68–0.905 Å; 0.935–1.6 Å.
Exposures:	at 9 different crystal orientations with PHIY/PHI = 0/0; 17/0–78.7°.

Number of predicted reflections		Number of processed reflections	
Total	150.997	'GOOD'	37.669
Useful	119.357	'WEAK'	45.623
Omitted		'BAD'	31.425
overlaps	28.854	'TOO DARK'	4.525
partials	2.786		

Symmetry R factors

Equivalent reflections within a given exposure:
$R_{sym} = 8.1$ to 12.8% (on I)
Equivalent reflections occurring on different exposures:
$R_{merge} = 10.9\%$ (on I) for GOOD reflections to 1.5 Å resolution (31.745 reflections, 14.488 unique; completeness 40% at 1.5 Å, 59% at 1.8 Å resolution)
$R_{merge} = 14.1\%$ for GOOD and WEAK reflections to 1.5 Å resolution (62.422 reflections, 23.822 unique; completeness 66% at 1.5 Å, 69% at 1.8 Å resolution)

Crystallographic R factor

$R_{cryst} = 24.3\%$ after three cycles of *EREF* refinement

crystal orientation (Koelln, 1990). Such zonal curves may easily be identified through the absence of reflection spots in the vicinity of the intense reflections along the curves. The direction cosines between a number of different zone axes were derived from the observed pattern and on the basis of the approximately known cell constants compared to theoretically possible values corresponding to low-indexed zones. Thus, the zone axes were indexed and hence the crystal orientation derived. Such procedures, which may also be extended to the case of unknown cell dimensions, have previously been described in the literature (Amoros, Buerger & Amoros, 1975; Vriend & Rossmann, 1987).

Spot integration

Spot integration employed a 'best-fit ellipsoid' procedure (Wilkinson, Khamis, Stansfield & McIntyre, 1988) modified for the case of a fixed crystal orientation; this procedure determines an envelope with an optimum ratio $I/\sigma(I)$. Starting from arrays of up to 21×21 pixels around the predicted spot positions, the program derived empirical masks with a typical size of 13×13 pixels for 16 different detector sections. An averaged elliptical model for the spot shape was obtained from successfully integrated ('GOOD') reflections. An alternative spot integration procedure was employed in test runs using a modified 'dynamical mask' (Sjölin & Wlodawer, 1981); this led to masks of slightly smaller sizes. However, the elliptical fit option yielded a significantly higher percentage of successfully integrated ('GOOD') reflections.

To check the efficiency of the spot integration routine, the reflection spots which were observed on one Laue exposure were compared to the predicted and successfully integrated spots. Fig. 3 shows part of this Laue exposure after digitization (*a*), together with the successfully integrated reflections (*b*) and the total predicted pattern (*c*). The comparison demonstrated that in fact all reflection spots which were just visible to the eye in the experimentally obtained exposure were successfully integrated.

Derivation of structure amplitudes

Structure-factor moduli, $|F(hkl)|$, were derived from the integrated reflection intensity, $I(hkl)$, according to (Zachariasen, 1945)

$$I(hkl) = I_0 Q \, \mathrm{d}V$$
$$Q = (e^2/mc^2 V_{uc})^2 PL|F(hkl)|^2$$

where I_0 is the incident intensity, $\mathrm{d}V$ the crystal volume, V_{uc} the volume of the unit cell, P the polarization factor (Kahn, Fourme, Gadet, Janin, Dumas & André, 1982) and L the Lorentz factor,

$$L = \lambda^4/\sin^2\theta.$$

Due to the broad wavelength bandwidth in the incident beam and the highly ordered crystal lattice, most of the simultaneously occurring reflections were fully excited; therefore, partials were omitted from further processing. A method to derive structure amplitudes from partially integrated Laue spots has been described elsewhere (Bartsch, Bartunik, Hohlwein & Zeiske, 1990, 1992).

Wavelength scaling

The Laue data were processed to 1.5 Å resolution for a wavelength range $0.63 < \lambda < 1.80$ Å. The numbers of predicted and processed reflections are listed in Table 1 for the BPT-TP 9 structure. To avoid a systematic bias of the results through misindexing of spots (occurring mainly at very short wavelengths) or by absorption effects at long wavelengths, only reflection spots excited by wavelengths within the range 0.70–1.60 Å were included in the further calculations. The entire set of structure factors was subdivided into 0.05–0.1° wide wavelength bins. Reflections which were omitted originated from wavelengths within 0.015–0.025 Å of the K-absorption edges of Br and Ag contained in the photographic films.

Bin-to-bin scaling factors were derived empirically from a comparison of equivalent reflections in different wavelength bins using scaling routines included in the program package *PROTEIN* (Steigemann, 1974). The bin-to-bin scaling of the Laue structure amplitudes actually involved two steps. In a first prescaling step, the overall scale factors of the individual wavelength bins were fitted to a theoretical curve corresponding to a predicted wavelength dependence. The prescaled structure

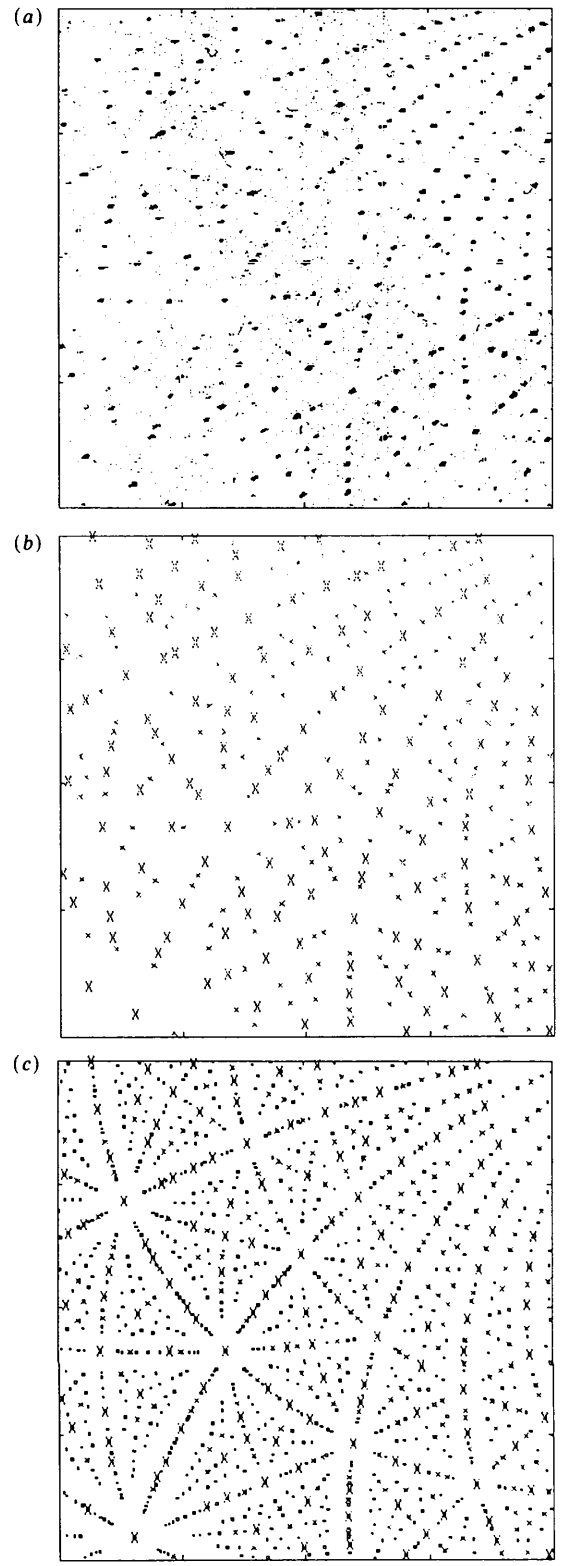

Fig. 3. Efficiency of Laue spot integration. (*a*) Experimentally observed spots (TP9) within an array of 512×512 pixels after digitization; (*b*) processed GOOD reflections [×] and overlapping spots [×]; (*c*) same as (*b*) plus all other predicted reflections.

amplitudes were loaded into *PROTEIN* for further bin-to-bin scaling. This repeated scaling procedure yielded slightly higher accuracy in the structure amplitude set characterized by an improvement in the merging R factor by 1–2% as compared to the first (prescaling) step. In theory, an overall B factor may be refined for each wavelength bin; however, we preferred to refine only scaling factors. The resulting bin-to-bin scaling-factor distribution is shown in Fig. 4. A merging R factor of 10.9% was obtained for the entire set of structure factors.

The shapes of the wavelength-scaling curves derived using the empirical procedures described above are compared in the following to a theoretical estimate of the wavelength dependence in the structure amplitudes. For a given reflection, the wavelength dependence in the structure-factor modulus is essentially contained in the relationship

$$|F| \propto I(\lambda)/\lambda.$$

The experimentally observed reflection intensity contains a number of wavelength-dependent factors,

$$I(\lambda) \propto S(\lambda) \exp[-Z_1(\lambda)]\{1-\exp[-Z_2(\lambda)]\}.$$

$S(\lambda)$ describes the intensity variation with wavelength in the incident synchrotron beam. The second term corresponds to a transmission factor taking into account absorption along the paths of the incident and diffracted beams.

$$Z_j(\lambda) = \sum_i \mu_{i,j} t_i \simeq \sum_i t_i (C_{ij}\lambda^3 - D_{ij}\lambda^4).$$

μ_i is the mass attenuation coefficient of an absorber i, t_i its thickness. The wavelength dependence of the mass attenuation coefficient may be expressed using the empirical formula of Victoreen (*International Tables for X-ray Crystallography*, 1985). The constants C and D relate to a given element and wavelengths between two absorption edges. The third term corresponds to the quantum detection efficiency. The wavelength dependence of Z_2 may be expressed in the same way as for Z_1.

On X31/DORIS, absorption along the incident and diffracted beam paths occurs mainly in the Be windows (total thickness *ca* 1.5 mm) containing Fe as an impurity (assumed to be 100 in 10^6), along air paths (total length about 30 cm), in the sample crystal and the surrounding solvent (total thickness about 0.8 mm) and the capillary tube (total wall thickness 0.02 mm). The corresponding Victoreen constants C and D were derived from tabulated total X-ray cross sections (*Handbook of Chemistry and Physics*, 1976) for wavelengths below the Fe K edge (at 1.743 Å). For an estimate of the quantum detection efficiency of photographic film, Victoreen constants were used for the wavelength range between the K edges of Ag (0.486 Å) and Br (0.920 Å) and for wavelengths above the Br K edge. The variation in the incident syn-

chrotron-radiation intensity with wavelength on a bending magnet at DORIS was taken into account (Pflüger & Gürtler, 1989). The reflectivity of a double-focusing mirror on X31 was assumed to be independent of the wavelength above the short-wavelength cutoff (at 0.6 Å); this neglects absorption near the L edge of the (Au) metal coating.

The theoretically estimated total wavelength dependence in $|F|$ is depicted in Fig. 4. At wavelengths above the Br K edge, there is good agreement with the empirical bin-to-bin scaling curve derived from the Laue data processing. At shorter wavelengths, the empirical scaling factors tend to be less reliable, mainly due to the lower accuracy in structure amplitudes. The good agreement over a broad range of wavelengths demonstrates the physical significance of the wavelength-scaling procedure.

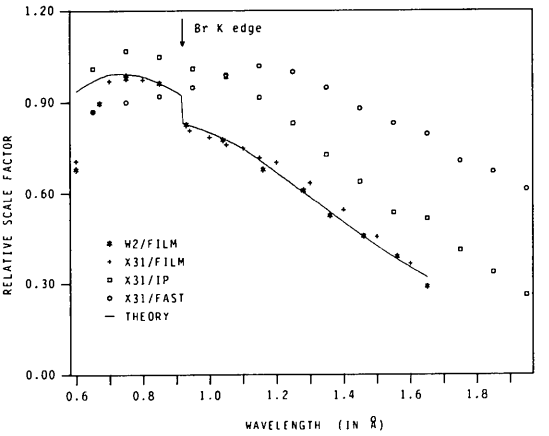

Fig. 4. Wavelength dependence in Laue structure factors derived by empirical bin-to-bin scaling of equivalent reflections for data collected on X31 (on film, image plate and FAST, respectively) and W2 (film). The curve corresponds to a theoretical estimate for W2 and film.

Completeness in Laue data as a function of resolution

The completeness in the Laue structure amplitudes varies as a function of $(\sin\theta)/\lambda$. This is shown in Fig. 2 for both TP 9 and HTN1 data. For comparison, a distribution typically obtained for monochromatic crystal rotation data is displayed for the example of DEBA structure factors (Marquart *et al.*, 1983). At high resolution, the distributions for Laue and for monochromatic structure factors are very similar. At low resolution, however, the Laue data are substantially less complete. Near the origin of reciprocal space, the volume contained between the limiting Ewald spheres is small; this explains the inefficiency of the Laue method to explore reciprocal space at low resolution. This lack of completeness affects the contrast in electron-density maps (see below).

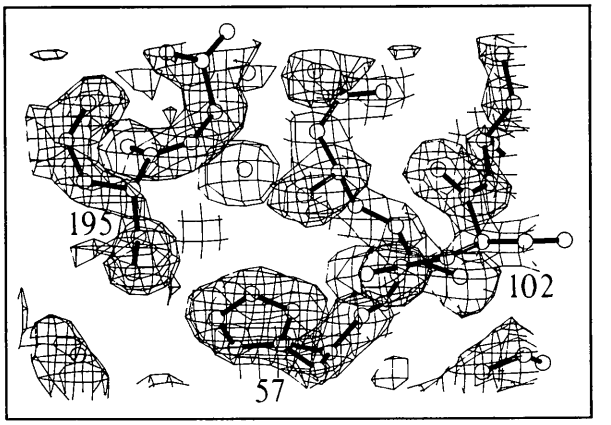

Fig. 5. $2|F_o|-|F_c|$ difference electron-density map of the active-site region of BPT calculated with a truncated monochromatic set of monochromatic DEBA structure factors. Contours are drawn at a 1σ level.

Crystallographic refinement

The BPT-TP 9 structure was refined on the basis of the Laue structure factors using start phases which were derived from the DEBA coordinates (Marquart *et al.*, 1983). A combined crystallographic- and energy-refinement protocol was employed using the program *EREF* (Jack & Levitt, 1978). Restraints were used for all atoms taking potential parameters from Levitt (1974). Unrestrained isotropic temperature factors of the individual atoms were refined with the *EREF* routines *DERIV* and *SHIFTS*. Structure factors were calculated with a program by S. J. Remington based on the FFT method by Ten Eyck (1977). Three cycles of both *EREF* and *B*-factor refinement were calculated.

The current R factor is 24% at 1.8 Å resolution. Despite the differences in the pH and the cell constants for TP 9 and DEBA, the refined structures are practically identical. The r.m.s. deviation between the positions of the backbone atoms is 0.10 Å; the maximum deviation amounts to 0.27 Å. Figs. 5 and 6 show examples of $2|F_o|-|F_c|$ electron-density maps

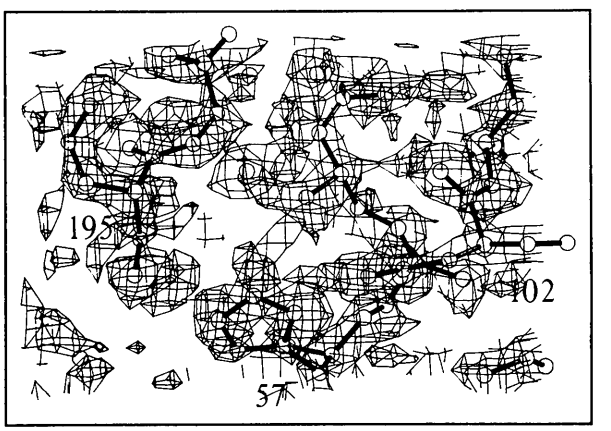

Fig. 6. $2|F_o|-|F_c|$ difference electron-density map calculated on the basis of TP 9 Laue structure-factor moduli and refined model phases. The second limits and contouring levels are the same as for Fig. 5.

which have been calculated from the refined TP9 coordinates and the experimentally derived Laue structure amplitudes.

Contrast in electron-density maps

Fig. 7 shows a section of a $2|F_o|-|F_c|$ difference Fourier map of BPT calculated at 1.8 Å resolution using Laue structure-factor moduli together with phases derived from the known structural model at pH 8.0 (DEBA; Marquart *et al.*, 1983). The loss in contrast in the 'Laue' map (Fig. 7*b*) as compared to the map calculated with both F_{obs} and phases from DEBA (Fig. 7*a*) is essentially due to the lack of low-resolution reflections in the Fourier synthesis and not to the slightly lower accuracy in Laue structure amplitudes. This is demonstrated by a comparison between the maps calculated from the complete set of DEBA-F_{obs} (Fig. 7*a*) and from a truncated set of DEBA-F_{obs} (Fig. 7*c*). The truncated DEBA set contains the same reflections as the Laue structure-amplitude set. As a further test, a small number (191) of randomly selected low-resolution model structure amplitudes F_{calc} were added to the Laue structure-amplitude set. A map (Fig. 7*d*) calculated from this combined set of F_{calc} and Laue structure amplitudes shows a high contrast comparable to that of the DEBA map.

Discussion

The accuracy in structure amplitudes derived from Laue diffraction measurements is affected by a number of different errors which are characteristic for the polychromatic excitation conditions. The main differences from monochromatic techniques arise

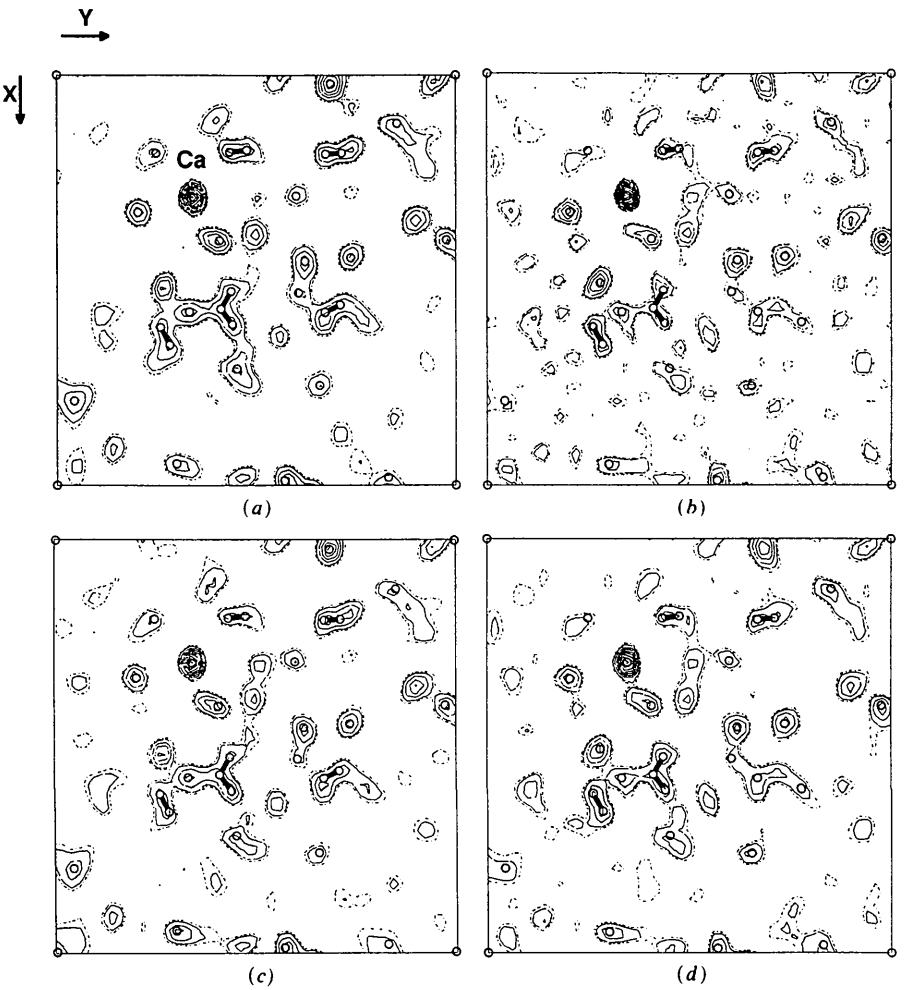

Fig. 7. Contrast in $2|F_o|-|F_c|$ difference Fourier maps calculated with (*a*) the entire set of monochromatic DEBA structure factors; (*b*) TP9 Laue structure-factor moduli and DEBA phases; (*c*) a truncated set of DEBA structure amplitudes containing the same reflections as the TP9 data; (*d*) TP9 structure amplitudes plus 191 randomly selected model structure amplitudes corresponding to low resolution (7–4 Å). All maps show the same section of a layer perpendicular to the *c* axis which contains the calcium binding site. Contours are in 1σ increments starting at 1σ. The dashed-dotted lines correspond to $0.8\ \sigma$.

from the dense population of reflections in Laue patterns, the reduced signal-to-noise ratio due to the wider bandwidth of exciting wavelengths, the influence of crystal mosaicity, and imperfect corrections for wavelength-dependent effects. The quality of electron-density maps calculated on the basis of Laue structure amplitudes is further affected by a systematic lack of completeness in the structure-amplitude set.

An increasing number of spatial overlaps and misindexing of reflections due to small spatial distances between neighbouring spots in a Laue diffraction pattern limit applications to low or medium resolution in the case of large cell dimensions. For a structure with cell dimensions <100 Å, such as BPT, Laue film data may be processed to essentially the same (very high) resolution as monochromatic crystal rotation exposures. The elliptical profile fitting method used in *LAUEMAD* requires a minimum area of about 3×3 pixels around each reflection spot. Under such conditions, the spot identification and integration routines work with high efficiency as indicated by the results obtained for BPT; successful processing of essentially all reflection spots which are visible to the eye is in fact a quite strict criterion.

Laue diffraction patterns show a smooth but intense background due to incoherent elastic and inelastic scattering from the sample and its immediate environment which originates from the entire range of incident wavelengths. The coherent scattering in a given Bragg reflection corresponds to a wavelength bandwidth which is two to three orders of magnitude smaller than the incident bandpass (of 1–1.5 Å in 'white-beam' Laue exposures). As a consequence, the accuracy of weak structure amplitudes is very substantially affected. The apparent diffraction limit is in general extended to larger d spacings; it degrades considerably with increasing molecular weight per asymmetric unit. Further, the diffraction limit is a function of the exciting wavelength; neglecting this wavelength dependence results in enhanced misindexing at high resolution and an even further reduction in the completeness at low resolution.

Even under white-beam excitation conditions, the set of structure amplitudes which may be measured from a stationary sample crystal will remain incomplete, at least for orthorhombic and lower-symmetry space groups. The example of orthorhombic space groups is relevant for a considerable percentage of all proteins crystallized up to now. In the case of orthorhombic BPT, the maximum completeness obtainable from any one exposure does not exceed 50% at high resolution. The situation is even worse at low resolution; the lack of completeness of the data set at low resolution is a systematic drawback of (stationary) Laue as compared to crystal rotation methods. The test calculations for the BTP structure demonstrate that this lack of completeness, which remained even for data measured at several different crystal orientations, caused a significant reduction in the contrast in electron-density maps. The polypeptide chain of BPT could still be traced unambiguously because the phases were known rather accurately; nevertheless, the exact location of a considerable number of side-chain atoms and water molecules was uncertain.

Applications aimed at a reliable determination of interatomic distances will for these reasons generally require Laue exposures at a number of different orientations involving rotation of the crystal around more than one axis, at least for space groups of orthorhombic and lower symmetry. For broadened crystal mosaicities and hence reduced wavelength bandwidths, the number of different crystal orientations must further increase. The aim of high completeness of data thus severely limits the time scales which may be reached in time-resolved studies of noncyclic reactions in the protein crystal.

The accuracy in protein structure analysis based on Laue data may be improved by including additional structural information derived from direct methods of phase extension. Despite the fact that Laue methods do not fully sample reciprocal space, particularly not at low and medium resolution, phase determination and expansion may be achieved with maximum-entropy methods (Bricogne, 1984; Bricogne & Gilmore, 1990) which appear to be less dependent on data quality, sampling and resolution than conventional direct methods (Gilmore, Bricogne & Bannister, 1990).

Concluding remarks

Laue diffraction methods yield structure-factor moduli which are sufficiently accurate for crystal structure analysis of proteins at high resolution. Compared to reflection intensities measured by monochromatic diffraction techniques, Laue data are generally less accurate due to a reduced signal-to-noise ratio and systematic errors caused by imperfect correction of wavelength-dependent effects. For orthorhombic structures, Laue methods sample reciprocal space inefficiently at low resolution. As a consequence, the contrast in electron-density maps calculated on the basis of Laue structure-factor moduli and (highly accurate) model phases is on average significantly poorer than in typical monochromatic studies. This lack in contrast is primarily due to the lack of completeness in Laue data; their lower accuracy appears to be of less importance. Therefore, the contrast varies greatly within the asymmetric unit.

If Laue data to high resolution from different crystal orientations and high-quality model phases are available, combined energy and crystallographic refinement of an orthorhombic structure of the size of BPT leads to meaningful results, despite a lack of

completeness of data. To achieve high contrast in electron-density maps, for instance in studies of small-amplitude conformational changes, either additional structural information must be available or modified data collection strategies must be followed which involve Laue exposures at even more crystal orientations or a combination of Laue and monochromatic crystal rotation techniques.

We are grateful for synchrotron beam time granted by the EMBL Outstation Hamburg on the instrument X31 and by DESY/HASYLAB on the wiggler station W2. This work has been funded by the German Federal Minister for Research and Technology (BMFT) under contract no. 05 180MP B 0.

References

AMOROS, J. L., BUERGER, M. J. & AMOROS, M. C. (1975). *The Laue Method.* New York: Academic Press.
BARTSCH, H. H., BARTUNIK, H. D., HOHLWEIN, D. & ZEISKE, T. (1990). *Acta Cryst.* A**46**, C21.
BARTSCH, H. H., BARTUNIK, H. D., HOHLWEIN, D. & ZEISKE, T. (1992). In preparation.
BARTUNIK, H. D. (1983). *Nucl. Instrum. Methods*, **208**, 523-533.
BARTUNIK, H. D. (1991). In *Handbook on Synchrotron Radiation*, Vol. IV, edited by H. EBASHI, M. H. J. KOCH & E. RUBENSTEIN. Amsterdam: North-Holland.
BARTUNIK, H. D. & BORCHERT, T. (1989). *Acta Cryst.* A**45**, 718-726.
BARTUNIK, H. D., FOURME, R. & PHILLIPS, J. C. (1982). In *Uses of Synchrotron Radiation in Biology*, edited by H. B. STUHRMANN. London: Academic Press.
BARTUNIK, H. D., SUMMERS, L. J. & BARTSCH, H. H. (1989). *J. Mol. Biol.* **210**, 813-828.
BODE, W. & SCHWAGER, P. (1975). *J. Mol. Biol.* **98**, 693-717.
BORCHERT, T. (1989). Diploma thesis, Univ. Hamburg, Germany.
BRICOGNE, G. (1984). *Acta Cryst.* A**40**, 410-445.
BRICOGNE, G. (1986). In Proc. of the EEC Cooperative Workshop on Position-Sensitive Detector Software (Phase III), LURE, Orsay, France.
BRICOGNE, G. & GILMORE, C. J. (1990). *Acta Cryst.* A**46**, 284-297.
CRUICKSHANK, D. W. J., HELLIWELL, J. R. & MOFFAT, K. (1987). *Acta Cryst.* A**43**, 656-674.
GILMORE, C. J., BRICOGNE, G. & BANNISTER, C. (1990). *Acta Cryst.* A**46**, 297-308.
HAJDU, J., ACHARYA, K. R., STUART, D. I., BARFORD, D. & JOHNSON, L. N. (1988). *Trends Biol. Sci.* **13**, 104-109.
HAJDU, J. & JOHNSON, L. N. (1990). *Biochemistry*, **29**, 1669-1678.
Handbook of Chemistry and Physics (1976). 56th ed., edited by R. C. WEAST, pp. E-139-143. Cleveland: CRC Press.
HELLIWELL, J. R. (1985). *J. Mol. Struct.* **130**, 63-91.
International Tables for X-ray Crystallography (1985). Vol. IV. Birmingham: Kynoch Press. (Present distributor Kluwer Academic Publishers, Dordrecht.)
JACK, A. T. & LEVITT, M. (1978). *Acta Cryst.* A**34**, 931-935.
KAHN, R., FOURME, R., GADET, A., JANIN, J., DUMAS, C. & ANDRÉ, D. (1982). *J. Appl. Cryst.* **15**, 330-337.
KOELLN, I. (1990). Diploma thesis, Univ. Hamburg, Germany.
LAUE, M. VON (1960). *Röntgenstrahlinterferenzen.* Frankfurt am Main: Akademische Verlagsgesellschaft.
LEVITT, M. (1974). *J. Mol. Biol.* **82**, 393-420.
MARQUART, M., WALTER, J., DEISENHOFER, J., BODE, W. & HUBER, R. (1983). *Acta Cryst.* B**39**, 480-490.
MESSERSCHMIDT, A. & PFLUGRATH, J. W. (1987). *J. Appl. Cryst.* **20**, 306-315.
MOFFAT, K. (1989). *Ann. Rev. Biophys. Biophys. Chem.* **18**, 309.
MOFFAT, K., SZEBENYI, D. & BILDERBACK, D. (1984). *Science* **223**, 1423-1425.
PFLÜGER, J. & GÜRTLER, P. (1989). Report SR-89-02. DESY, Hamburg, Germany.
REEKE, G. N. (1984). *J. Appl. Cryst.* **17**, 238-243.
SCHLICHTING, I., RAPP, G., JOHN, J., WITTINGHOFER, A., PAI, E. F. & GOODY, R. S. (1989). *Proc. Natl Acad. Sci. USA*, **86**, 7687.
SJÖLIN, L. & WLODAWER, A. (1981). *Acta Cryst.* A**37**, 594-604.
STEIGEMANN, W. (1974). PhD thesis, Technische Univ. München, Germany.
TEN EYCK, L. F. (1977). *Acta Cryst.* A**33**, 486-492.
VRIEND, G. & ROSSMANN, M. G. (1987). *J. Appl. Cryst.* **20**, 338-343.
WILKINSON, C., KHAMIS, H. W., STANSFIELD, R. F. D. & MCINTYRE, G. J. (1988). *J. Appl. Cryst.* **21**, 471-478.
ZACHARIASEN, W. H. (1945). *Theory of X-ray Diffraction in Crystals.* New York: Wiley.

Acta Cryst. (1992). A**48**, 188-197

On the Mapping of Electrostatic Properties from the Multipole Description of the Charge Density

BY ZHENGWEI SU AND PHILIP COPPENS

Chemistry Department, SUNY at Buffalo, Buffalo, NY 14214, *USA*

(*Received* 18 *March* 1991; *accepted* 12 *August* 1991)

Abstract

A method is presented to calculate the electrostatic potential, the electric field and the electric-field gradient in a crystal from the atomic multipole expansion of the experimental charge density, as described by the Hansen-Coppens formalism [Hansen & Coppens (1978), *Acta Cryst.* A**34**, 909-921]. The electrostatic properties are expressed in terms of the positions and the charge-density parameters of the individual atoms. Contributions due to the procrystal charge density and the deformation

0108-7673/92/020188-10$03.00